

# Dynamic Performance Comparison between Buckling-Restrained Braced Frames in Concentric and Eccentric Configurations



**G.S. Prinz**

*Steel Structures Laboratory (ICOM), École Polytechnique Fédérale de Lausanne (EPFL),  
Lausanne, Switzerland*

**P.W. Richards**

*Dept. Civil and Environmental Engineering, Brigham Young University, USA*

## **SUMMARY:**

The ductility of buckling-restrained braced frames (BRBFs) can be limited by poor performance of the beam-column-gusset regions. Additionally, the concentric brace configuration in BRBFs can limit the use of architectural features. BRBFs with braces in eccentric configurations (called BRBF-Es) may accommodate architectural features similar to eccentrically braced frames, and limit damage to the connection regions through 1) the use of beam splices and 2) separation of the column-to-gusset connection which prevents pinching of the brace gusset plate. In this study, the system-level and component-level dynamic performances of conventional BRBF systems are compared with those of BRBF-E systems. Multi-directional dynamic analyses are performed on 5-story BRBF and BRBF-E systems to compare drift demands and local connection demands. Results indicate similar stiffness between the BRBF and BRBF-E systems; however, with the BRBF-E, gusset connection stresses are reduced due to the beam splices and eccentricity between the brace connection and column.

*Key Words: BRBF-E; Dynamic Nonlinear Analysis; Earthquake Loads; Shell Elements*

## **1. INTRODUCTION**

In concentric buckling-restrained braced frames (BRBFs), braces often interfere with architectural features, and the performance of brace connection regions often limits the entire system ductility. Multiple experimental studies on concentric BRBFs demonstrate limited ductility at low drifts due to out of plane distortion of the brace gussets and fracture of the gusset-to-beam or gusset-to-column welds (Aiken et al., 2002; Chen et al., 2004; Roeder et al., 2006). This poor connection performance has been attributed to gusset-plate pinching caused by relative deformations between the beam and column joint. The use of beam splices (Coy, 2007; Fahnestock et al., 2007; Prinz and Richards, 2008) and eccentric configurations with detached-column connections may help prevent such connection issues while allowing architectural features such as doors, windows or halls.

BRBFs with braces in eccentric configurations (called BRBF-Es) could combine the architectural benefits of eccentrically braced frames (EBFs) with the design and performance benefits of concentric BRBFs. BRBF-Es could accommodate architectural features using brace eccentricities similar to EBFs, while dissipating seismic forces through axial yielding of the braces, similar to concentric BRBFs.

A recent study by Prinz and Richards (2012) demonstrated similar dynamic performance between BRBF-E systems and typical EBF systems. In Prinz and Richards (2012), multiple BRBF-E and EBF designs were subjected to multiple scaled earthquake motions. Results indicated similar peak inter-story drift demands between the two frame types, with the BRBF-Es performing slightly better than the EBFs. While the study by Prinz and Richards (2012) sheds insight into global performance of BRBF-Es, the modeling techniques used prevent determination of localized performance near connection regions.

In this study, three-dimensional finite element models with shell elements are used to compare the system and component performance of BRBF-Es with typical BRBFs under multi-directional dynamic loads. The paper begins with a description of the BRBF control structure used to validate the various finite element modeling techniques. Following, the techniques used to model the control structure are described, and two BRBF-E test models are discussed. Lastly, results from multi-directional dynamic loading of the control model and test models are presented, and BRBF-E connection demands are quantified and discussed.

## 2. BRBF CONTROL STRUCTURE

A 5-story BRBF building designed and dynamically tested at the E-Defense Hyogo Earthquake Engineering Research Center in Tokyo, Japan, was used to validate analytical models with experimental result (Kasai et al., 2010). The building incorporated BRBs in both directions and was constructed having concrete slabs at each floor. The bay dimensions, and floor weights for the E-defense structure are given in Figure. 1. Dynamic loading of the test structure is discussed in a later section.

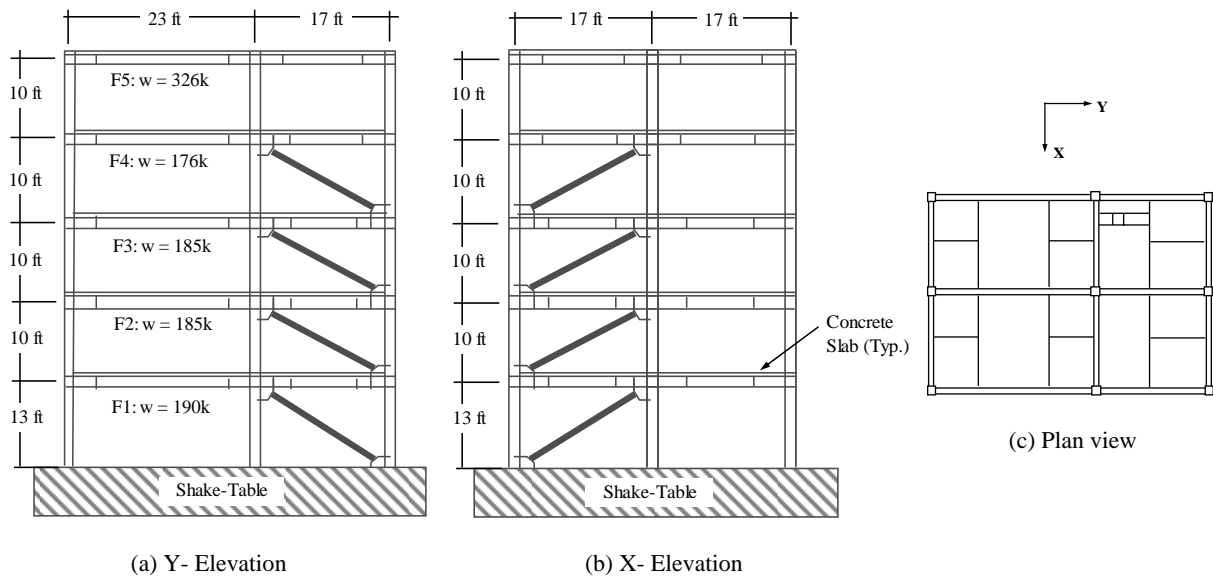


**Figure 1.** Floor weights and frame dimensions for E-Defense test structure

### 2.1. Modeling Methods for Control Structure

A control model simulated the test setup and dynamic loading used by the 5-story test structure. The control model was considered as a 3-dimensional system using ABAQUS (HKS, 2006). Due to lack of symmetry in the structure, the entire geometry was considered in the analysis. Figure 2(a) shows the 3-dimensional control model. The base of the gravity columns in the control model were assumed pinned, while the base of the seismic frames were assumed fixed. Floor masses were lumped at each column based on tributary floor area. Rather than incorporate rigid diaphragm constraints to transfer mass between the columns, the concrete slabs were explicitly modeled.

Mesh size and element type affect the accuracy of analysis. The control model used four-node linear quadrilateral elements at a general mesh size of 152mm (6in.). In regions of interest, regions with the highest potential for local buckling and stress concentrations, the mesh size was reduced to 76mm (3in.) for improved strain accuracy. The mesh refinement was implemented near the connection regions, along

the beams, and at the edges of the concrete slabs. In regions of little interest, near the middle of the concrete slab, the mesh was coarsened to an element size of 381mm (15in.). The meshed model resulted in 131,959 elements. Figure 2(b) shows the meshed control model.

Five percent stiffness proportional damping was specified in the first mode. All mass proportional damping was neglected. Equation 2.1 was used to calculate the stiffness proportional damping coefficient,  $\beta$ , used in the ABAQUS analysis:

$$\beta = \frac{2 \cdot \zeta}{\omega_i} \quad (2.1)$$

In Equation 2.1,  $\omega_i$  and  $\zeta$  are the frequency at a given mode and damping ratio respectively.

To obtain the fundamental modes of vibration and natural frequencies used to calculate  $\beta$ , frequency analyses were conducted. Figure 3 shows the frequency results for the first two modes of vibration of the control model, with corresponding natural frequencies. Considering five percent damping in the first mode,  $\beta$  of the control model was calculated as 0.0086.

For all beams, columns, and gussets, non-linear material properties and large displacement effects were considered in the analyses. Material plasticity for all beams, columns, and gussets was based on a von Mises yield surface and an associated flow rule. Plastic hardening was defined using a nonlinear kinematic hardening law. Steel coupon tests from the E-defense structure were used to calibrate the material parameters in the model. Large displacement effects allowed for local member buckling, and were accounted for using the nonlinear geometry option in ABAQUS.

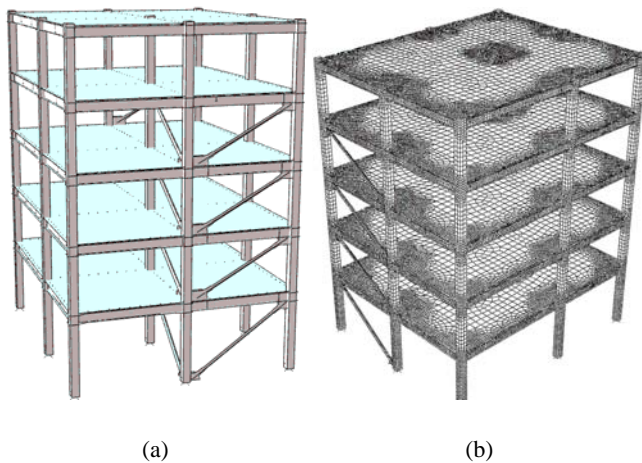


**Figure 2.** (a) 3-dimensional ABAQUS control model of E-Defense test structure; and, (b) typical model mesh

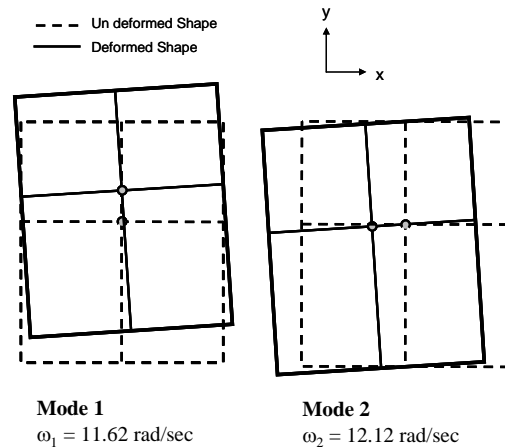


**Figure 3.** First and second vibration modes for BRBF control model.

## 2.2. Buckling-Restrained Brace Specific

The buckling-restrained braces were explicitly modeled using shell elements. To simulate confinement of the brace core and prevent the brace from buckling out of plane, rotation constraints (both in and out of plane) were implemented along the brace core length. Based on a drift of 4%, the brace core was calculated to extend 100mm (4 in.) out of the confining material; therefore, the rotation constraints were not implemented within 50mm (2 in.) of the brace-gusset connection on either end. A multi-linear steel

constitutive model developed by Coy (2007) modeled the inelastic strength gain of the brace. Consistent with construction details provided by E-Defense, the brace-core yield strength was specified at 220MPa (32 ksi).

### 2.3. Concrete Slab Specific

Shell elements and equivalent concrete material properties modeled the concrete slab. Modeling for the concrete slab followed techniques similar previous studies on composite moment frames (Zhang et al., 2004; Zhou et al., 2007). Four-node isoperimetric shell elements located at the slab centerline defined the slab geometry. For simplicity, an elasto-plastic compression only constitutive model with reduced concrete modulus and yield strength defined the concrete material behavior (similar to Zhang et al. (2004) and Zhou et al. (2007)). Calibration of the concrete constitutive behavior is presented in Prinz (2010).

Load transfer between the concrete slab and steel beam in a composite frame is primarily achieved through embedded stud connectors. For this reason, the interaction between the concrete slab and steel beam was modeled as a discrete connection using two linear springs and nodal displacement constraints (see Figure 4). Two spring elements (SPRING2 in ABAQUS) were oriented in the longitudinal and transverse beam directions to simulate the shear stiffness of a typical stud connector. A constraint joining the beam and slab nodes restricted relative vertical movement. The stiffness of the linear springs was calculated using typical stud properties in Equation 2.2:

$$K_s = \frac{0.9 \cdot G_s \cdot A_s}{L_s} \quad (2.2)$$

where  $K_s$ ,  $G_s$ ,  $A_s$ , and  $L_s$  are the spring stiffness, shear modulus of a typical stud, stud cross-sectional area, and stud length respectively.

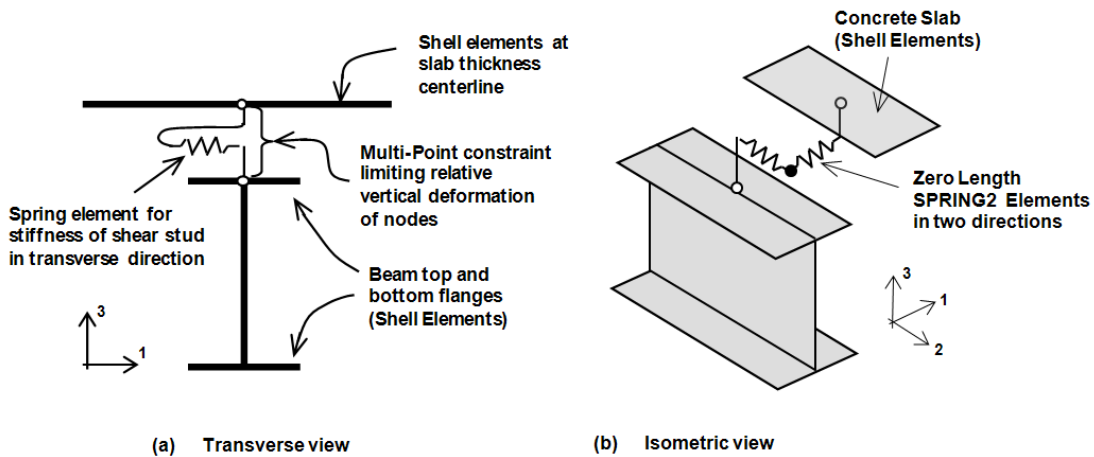


Figure 4. Modeling technique for discrete beam-to-slab connection

### 3. DESCRIPTION OF BRBF-E TEST MODELS

Two additional models with brace eccentricities and beam splices were analyzed, representing BRBF-Es. The two BRBF-E models were chosen to investigate the effects of different beam splice connection locations on gusset stresses. The same modeling techniques for the BRBF control model were used in the BRBF-E test models. The brace geometry for the BRBF-E models was modified slightly from the control

model, to form the eccentric brace connections. Additionally, brace areas in the BRBF-Es were modified to match the lateral story strength of the control model. Beam and column sizes were also modified from the control model, to ensure elastic response with the new brace geometry. Figure 5 shows the BRBF-E brace geometry for both test models.

The first BRBF-E model, hereafter referred to as model MSC (mid-splice connection), considers a beam splice connection in the middle of the beam, similar to the splice connection tested by Fahnestock et al. (2007). To model the mid-beam splice connection, beam nodes were rigidly constrained to a reference node at the middle of the beam, and tied to an adjacent reference node using a hinge multi-point constraint (see Figure 6(a)). Modeling this beam splice connection as a perfect hinge was validated by Prinz and Richards (2008).

The second BRBF-E model, hereafter referred to as model TSC (top-splice connection), used a beam splice connection at the top flange of the beam, similar to the connection tested by Coy (2007). Modeling the top-flange-splice connection is similar to that of the mid-splice connection; except reference nodes are located at the beam top flange (see Figure 6(b)).

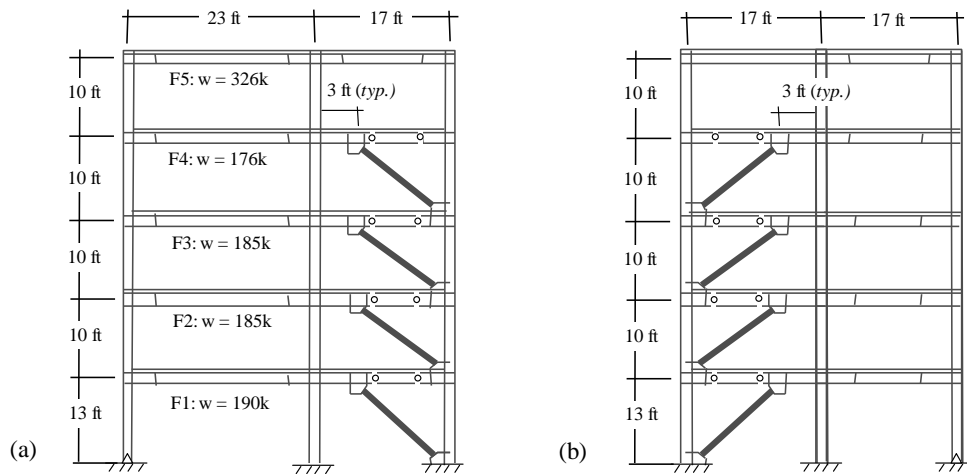


**Figure 5.** Test model frame geometry for: (a) frames in Y-direction; and, (b) frames in X-direction

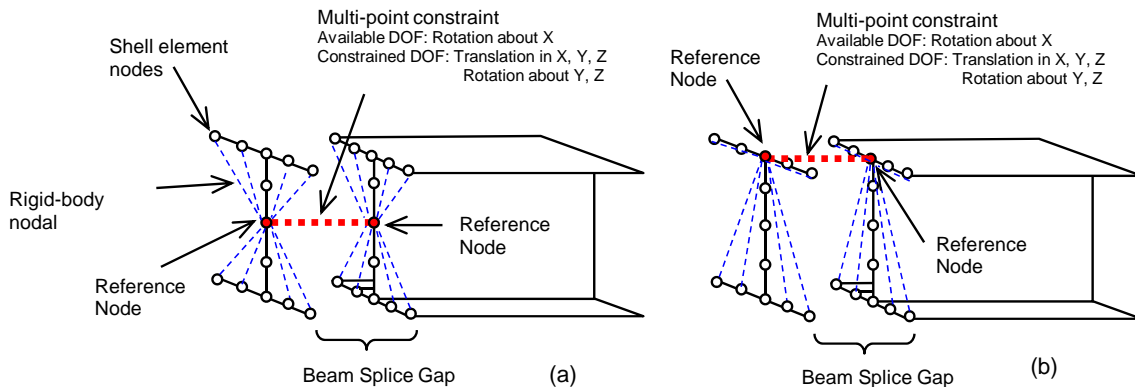


**Figure 6.** Modeling of hinged beam splice for: (a) mid-splice connection; and, (b) top-splice connection.

Since the presence of a beam splice and modified brace geometry have the potential to affect the model stiffness, new damping factors needed to be determined. Similar to the control model, frequency analyses were conducted on each BRBF-E model to determine the natural vibration frequencies. Considering five

percent damping in the first mode,  $\beta$  was calculated as 0.0086 for both models MSC and TSC (note that this is the same value calculated for the control model).

#### 4. FRAME LOADING

The E-defense test structure, ABAQUS control model, and BRBF-E test models were all dynamically loaded using accelerations derived from the 1995 Kobe earthquake (JR Takatori station). Acceleration components recorded in both the X- and Y-directions were applied simultaneously during analysis. An acceleration scaling of 1.0 times the recorded shake-table motion was used to directly compare the control model and BRBF-E models with the E-defense test.

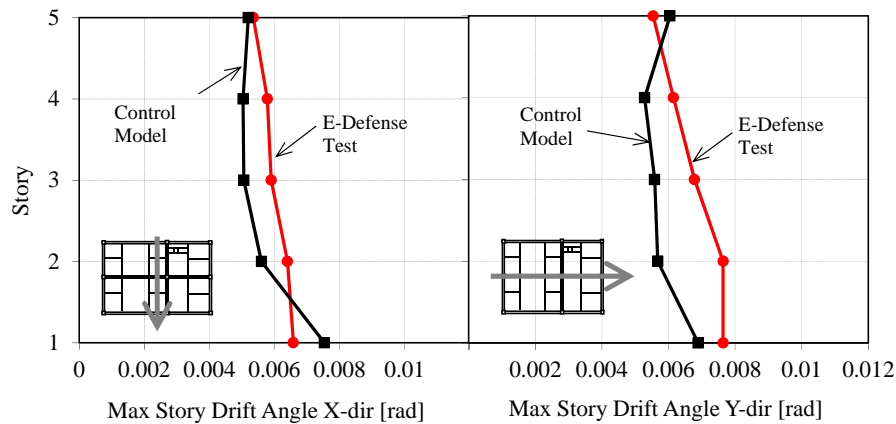
### 5. RESULTS

#### 5.1. Control Model Validation

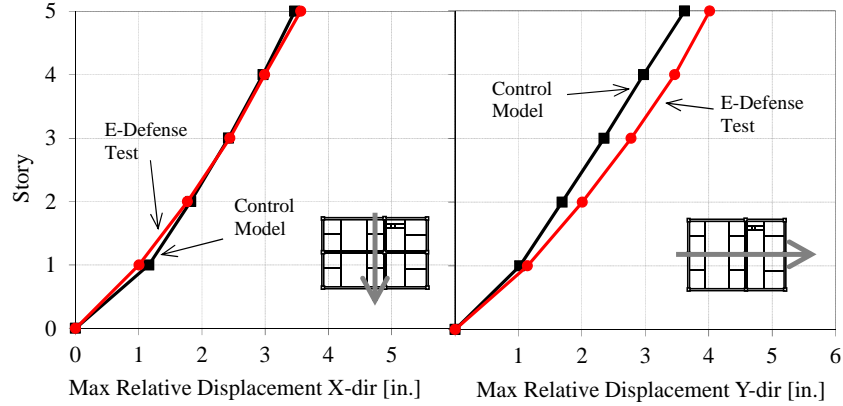
Comparisons of system and component responses (story drifts, displacements, and column strains) between the E-defense test and control model provide reasonable confidence in the modeling methods and analysis procedures.

Figure 7 and Figure 8 show the maximum absolute value of story drift and total relative story displacement respectively, for the E-defense test and control model. The control model X-direction story drift values were within 15% of the E-Defense test, and control model Y-direction story drift values were within 15% for stories 1, 3, 4, and 5, and within 25% for story 2. Slight drift discrepancies in the lower stories (within 25% for story 2) are partly due to the column-base boundary conditions assumed for the control model; the column-base fixity of the actual test was most likely in-between perfectly rigid and perfectly pinned.

Maximum X-direction story displacements between the test and control model differed by less than 2.5mm (0.1in.) at stories 2 through 5, and by less than 3.8mm (0.15in.) at the first story (see Figure 8). In the Y-direction, maximum story displacements between the test and control model differed by less than 12.7mm (0.5in.) at all stories.



**Figure 7.** Comparison of X-, and Y-direction inter-story drift between control model and E-Defense test (Kasai et al., 2010)



**Figure 8.** Comparison of X- and Y-direction relative story displacements for control model and E-Defense test (E-Defense, 2009)

## 5.2. Results for BRBF-E Test Models

### 5.2.1. Inter-Story Drift Angles

Inter-story drift values for the two BRBF-E test models and control model were similar in value. Maximum inter-story drift angles for models TSC, MSC, and the BRBF control model are shown in Figure 9. Story drifts between model TSC and MSC were within 4% in the X-direction, and within 16% in the Y-Direction. In the lower stories of the Y-direction frames, drift values for model MSC were slightly larger than those for model TSC and the control model (0.001rad larger at the base, see Figure 9). Drifts between the BRBF-E models and the control model were reasonably similar, with the largest difference occurring in the first floor of the X-direction frames. First floor X-direction drift for the control model was 0.002 rad larger than the drift for models MSC and TSC. The similarities in inter-story drift are somewhat expected, given the similar system frequencies (note the same stiffness proportional damping factor,  $\beta$ , determined from frequency analysis).

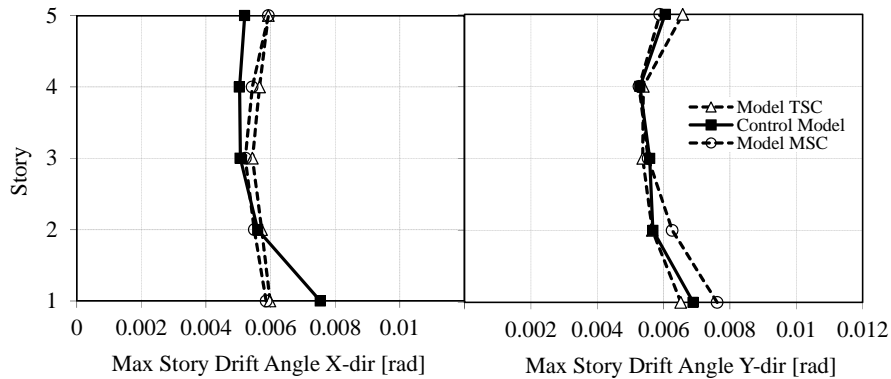


**Figure 9.** Comparison of X- and Y-direction story drift for model MSC, model TSC, and the control model

### 5.2.2. Beam-to-Column Connection Stresses

The distribution of flange stresses between the BRBF-E test models and control model indicated stress concentrations near the BRBF-E stub-to-column connection. Figure 10 shows the top-flange von Mises stress values for the control model and BRBF-E test models. From Figure 10, stress values near the flange-to-column connection of the BRBF-E models were higher than those of the control model. Flange

connection stresses for the BRBF-E models were 4.5 times larger, on average, than the control model for the X-direction frames, and nearly 6 times larger for the Y-direction frames. The BRBF-E flange stresses away from the column connection reduced to values similar to the control model (see Figure 10). The stress values were taken at the time-step corresponding to maximum frame displacement ( $time_{y-direction}=5.3\text{sec}$ ,  $time_{x-direction}=8.1\text{sec}$ ). The stress concentrations near the flange-to-column connections of the BRBF-E models are from the increased beam bending moment caused by the brace eccentricity. In EBFs, these flange-to-column stress concentrations lead to early connection failure through material fatigue (Okazaki et al., 2006); however, unlike EBF beams, the stubs of the BRBF-E models remained elastic, eliminating the possibility for low-cycle fatigue. With the BRBF control model, the concentric brace connection reduced the beam moment, resulting in lower flange-to-column connection stresses.

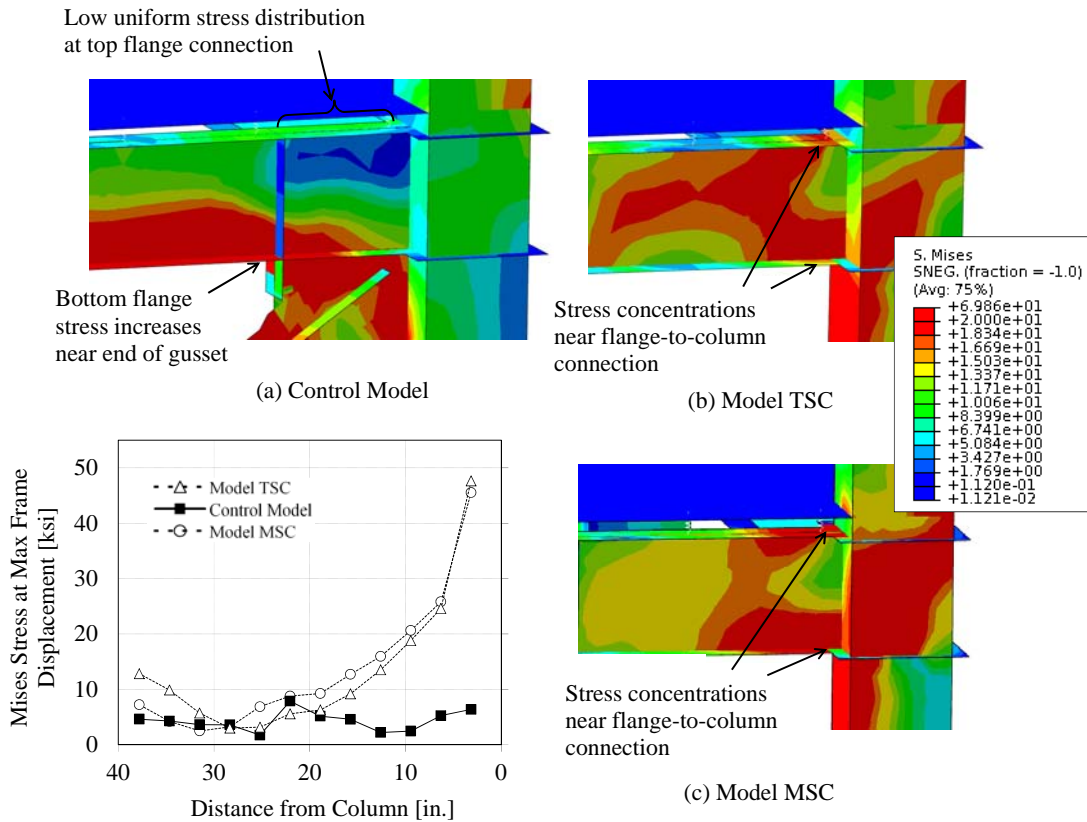


**Figure 10.** First-story beam-to-column connection stress contours in Y-direction frames for: (a) control model; (b) model TSC; and, (c) model MSC

### 5.2.3. Gusset Connection Stresses

Gusset-to-beam stress contours for the X-direction frames of models MSC, TSC, and the control model are shown in Figure 11. The gusset-to-beam contours for models MSC and TSC in Figure 11 are low and relatively uniform, with only a slight decrease in stress toward the beam splice, away from the column-edge of the gusset. The gusset-to-beam stress contours in the control model increased significantly away from the gusset column-edge (see Figure 11(a)). This increase in gusset stresses away from the gusset column-edge is explained by changes in the beam-to-column connection angle (pinching and expanding the gusset region).

The distribution of stress values in the top gusset-to-beam connection for models TSC, MSC and the control model is shown in Figure 11. The maximum gusset-to-beam stress values in the control model were near double those of the BRBF-E models (for the X-direction frames). As mentioned earlier, these larger gusset stresses in the BRBF-C control model are due to changes in the beam-to-column angle, resulting in pinching and expansion of the gusset plate. Since the BRBF-E models are only attached to the beams, changes in beam-to-column geometry have less effect on the BRBF-E gusset stresses. Gusset connection stresses for models MSC and TSC were similar in value, and rather uniform, in the X-direction frames. In the Y-direction frames, gusset-to-beam connection stresses for the control model and model TSC were similar and consistently higher than those for model MSC. This result may be due to slight brace-end and gusset plate distortions (brace-ends and gussets in the lower stories of model TSC slightly buckled out of plane).

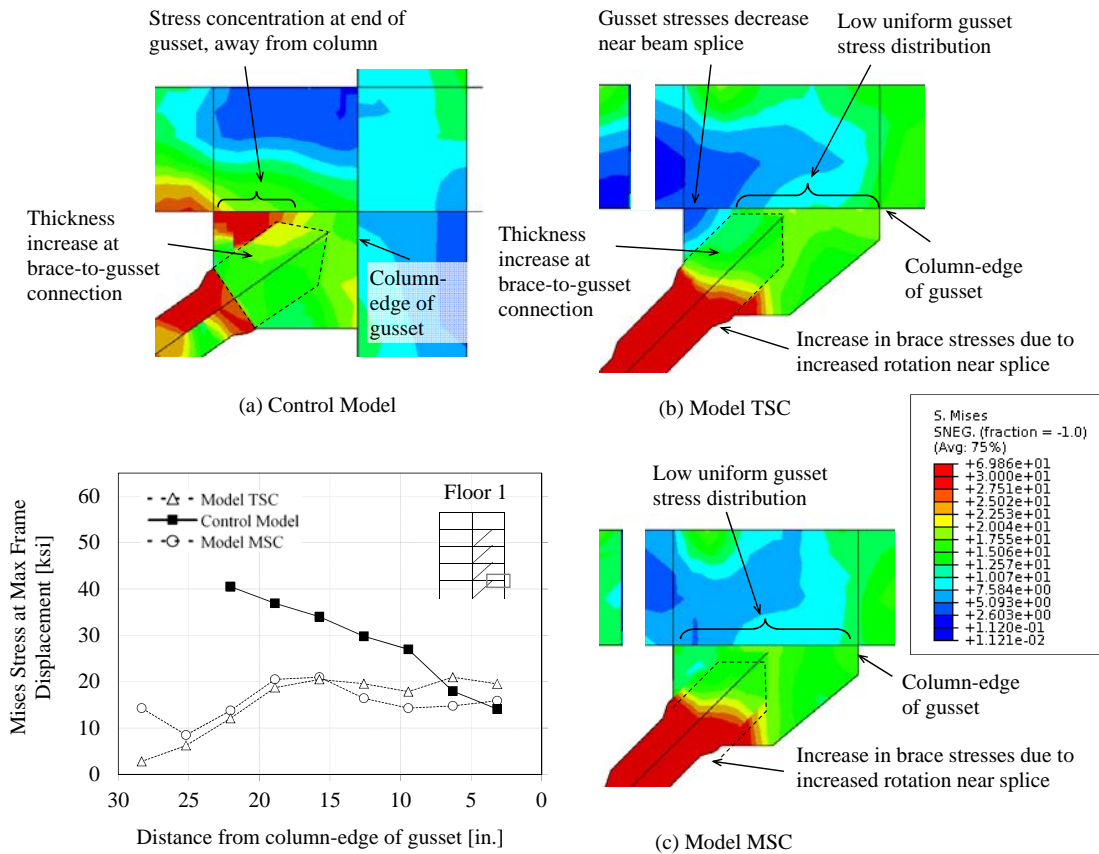


**Figure 11.** Gusset-to-beam stress contours for: (a) control model; (b) model TSC; and, (c) model MSC

## 6. SUMMARY AND CONCLUSIONS

In this paper, multi-directional dynamic loads were applied to three finite element models representing concentric BRBFs and BRBF-Es. The geometry of the finite element models was created using shell elements. The concentric BRBF model allowed for system-level validation of various modeling techniques, as well as comparison between BRBF and BRBF-E dynamic response. Two BRBF-E models were created with identical geometry, but different beam-splice connection types (top-flange and mid-splice connections), to help determine the effects of the beam splice location. The specific modeling techniques presented in the chapter included: modeling of the concrete slab, slab-to-beam connection, and

buckling-restrained brace. The modeling methods allowed for determination of component connection stresses and strains, as well as system-level frame response. The following conclusions are from the component and system response of the three computer models:

1. System-level frame response for concentric BRBFs and BRBF-Es are similar, with similar story strengths, indicating similar system stiffness. Modal frequencies between the concentric BRBF control model and BRBF-E test models were similar.
2. BRBF-E stubs have stress concentrations at the beam-to-column connection similar to EBF link-to-column connections; however, elastic stub responses eliminate material fatigue concerns. The BRBF-E stub stress concentrations were 4-6 times greater than those in the concentric BRBF beams.
3. Gusset-to-beam connection stresses for BRBF-Es are relatively uniform, and lower than those of the concentric BRBFs, when the brace-ends remain in-plane. The beam splices and eccentric location of the brace connections prevent gusset stress concentrations due to pinching and expansion of the beam-column joint (a common cause of failure in concentric BRBF configurations).

## REFERENCES

- Aiken, I. D., Mahin, S.A., and Uriz, P.R. (2002). "Large-scale testing of buckling restrained braced frames." *Proc. Japan Passive Control Symposium*, Tokyo Institute of Technology, Japan.
- Chen, C. H., Hsiao, P.C., Lai, J.W., Lin, M.L., Weng, Y.T., and Tsai, K.C. (2004). "Pseudo-dynamic test of full-scale CFT/BRB frame: Part 2 - Construction and testing." *Proc. 13th World Conference on Earthquake Engineering*, Vancouver, B.C., Canada, Paper No. 2175.
- Coy, B. B. (2007). "Buckling-restrained brace connection design and testing." *Masters Thesis*: Brigham Young University, Provo, UT.
- E-Defense (2009). Blind analysis contest application site, Website: [http://www.blind-analysis.jp/index\\_e.html](http://www.blind-analysis.jp/index_e.html).
- Fahnestock, L. A., Ricles, J.M., and Sause, R. (2007). "Experimental evaluation of a large-scale buckling-restrained braced frame." *J. Struct. Eng.*, 133(9): 1205-1214.
- HKS (2006). "ABAQUS Standard Users manual, Version 6.4." Hibbitt, Karlsson, and Sorensen, Inc.
- Kasai, K., Ito, H., Ooki, Y., Hikino, T., Kajiwar, K., Motoyui, S., Ozaki, H., and Ishii, M. (2010). "Full-scale shake table tests of 5-story steel building with various dampers." *Joint Proc. 7th International Conf. on Urban Earthquake Eng. and 5th International Conf. on Earthquake Eng.*: Tokyo, Institute of Technology, Tokyo, Japan.
- Okazaki, T., Engelhardt, M.D., Nakashima, M., and Suita, K. (2006). "Experimental performance of link-to-column connections in eccentrically braced frames." *J. Struct. Eng.*, 132(8): 1201-1211.
- Prinz, G. S. (2010). "Using buckling-restrained braced frames in eccentric configurations." *Ph.D. Dissertation*: Brigham Young University, Provo, Utah.
- Prinz, G. S., and Richards, P.W. (2008). "Seismic response of buckling-restrained braced frames with beam splices." *Proc. 14th World Conference on Earthquake Engineering*, Beijing, China.
- Prinz, G. S., and Richards, P.W. (2012). "Seismic performance of buckling-restrained braced frames with eccentric configurations." *J. Struct. Eng.*, 138(3): 1-9.
- Roeder, C. W., Lehman, D.E., and Chistopulos, A. (2006). "Seismic performance of special concentrically braced frames with buckling restrained braces." *Proc. 8th U.S. National Conf. on Earthquake Engineering*, San Francisco, CA, Paper No. 1503.
- Zhang, X., Ricles, J.M., Lu, L.-W., and Fisher, J.W. (2004). "Analytical and experimental studies on seismic behavior of deep column-to-beam welded reduced beam section moment connections." *13th World Conference on Earthquake Eng.*, Vancouver, B.C., Canada: Paper No. 1599.
- Zhou, F., Moslam, K.M., and Masayoshi, Nakashima (2007). "Finite-element analysis of a composite frame under large lateral cyclic loading." *J. Struct. Eng.*, 133(7): 1018-1026.